Metal-vapor production by sputtering in a hollow-cathode discharge: Theory and experiment[a)]

B. E. Warner and K. B. Persson
National Bureau of Standards, Boulder, Colorado 80303

G. J. Collins[b)]
Department of Electrical Engineering, Colorado State University, Fort Collins, Colorado 80523

(Received 27 February 1979; accepted for publication 4 May 1979)

Laser action in singly ionized metal atoms has been obtained when a rare gas is excited in a metal hollow cathode. The required metal-vapor density is produced by discharge sputtering from the cathode and the excitation of upper levels occurs via a charge-transfer reaction of the type $B^+ + M \rightarrow (M^+)^* + B + \Delta E$. We present a unified discharge-sputtering theory which describes the metal density created in the hollow cathode, including both the current and spatial dependence. The predictions of this model are then compared to the measured dependence of metal-vapor density with current, spatial position, and buffer-gas pressure. Discharge conditions which support laser oscillation are emphasized. Agreement between theory and experiment is good.

PACS numbers: 52.80.Hc, 79.20.Nc, 52.90. + z

I. INTRODUCTION

Cathode sputtering has been utilized to produce involatile metal densities of 10^{14} atoms/cm^3 in hollow-cathode laser tubes.[1] The resulting metal-ion laser transitions, pumped by charge transfer from rare-gas ions to metal-vapor atoms, span the 220–800-nm spectral range.[2–9] Several near-infrared transitions in Cu II and Ag II provide 1-W output power in simply designed sputtering hollow cathodes,[10] which operate at room temperatures. These lasers are unique in that the creation of metal atoms by sputtering depends upon the discharge conditions. Hence, a *unified* discharge theory including sputtering must be developed to characterize the behavior of these lasers.

We present a model of the sputtering mechanism in the hollow-cathode discharge, based on the presence of charge transfer as outlined in Sec. II B. This model is formulated to apply to buffer-gas pressures and discharge currents characteristic of the sputtering hollow-cathode lasers. It predicts the current dependencies of the metal-vapor density and the rare-gas ion density, as well as the spatial distribution of the metal vapor in the hollow cathode. This paper then compares available experimental data to the predictions of the sputtering model. Data and theory are shown to be in good agreement. Finally, conclusions are drawn from the model concerning the scaling laws and optimum operating conditions for the sputtering hollow-cathode lasers.

The presentation of our work is divided into two parts; one, the current dependence of the sputtered metal-vapor density, and two, the spatial variation of the metal density. In both cases experimental data and theoretical predictions are compared.

II. SIMPLIFIED DISCHARGE MODEL: METAL DENSITY VERSUS CURRENT

A. Description of the hollow-cathode discharge

Sputtering hollow-cathode lasers have been built with both cylindrical[3] and rectangular[11] hollow-cathode structures. In each case one-dimensional geometry is appropriate as a first approximation for discharge modeling as there is little or no variation in discharge parameters along the optical axis of these devices. The plasma is also approximately homogeneous in one other direction normal to the optical axis. In our work plane-parallel geometry is used, but it can be easily extended to the cylindrical case. Figure 1(a) shows a cross section of a rectangular hollow cathode with pertinent dimensions. The height h is assumed large enough so that the major part of the plasma is free of end effects. A schematic representation of the potential distribution from one cathode surface to the other is shown in Fig. 1(b). The plasma may be broken into two regions; a thin plasma sheath of width d ($d \ll a$), which hugs each cathode surface, and a relatively field-free negative-glow region with a space potential close to that of the anode. Note that the voltage drop across the sheath region nearly equals the full anode-cathode voltage.

The discharge can be thought of as being beam maintained. Electrons, leaving the cathode surface, are accelerated in the sheath region, obtaining energies up to the cathode-fall voltage V_c.[12] These beam electrons are trapped in the negative-glow region of the plasma, due to the potential well of depth V_c, and lose their energy in ionizing and exciting collisions with the buffer-gas atoms. In the sputtering hollow-cathode lasers, the discharge width is small enough ($2a = 2$–4 mm) so that, with operating pressures (500–1500 Pa $\simeq$ 4–12 Torr, He or Ne) the electron beam created in the sheath at 300 V possesses a reaching distance[13] longer than $2a$. Hence, the beam electrons will oscillate between opposing sheaths.[14]

This beam concepts provides the basis for our approximation of a spatially uniform source for electron-ion pairs throughout the negative glow. In other words, we will assume, to first order, that the source function S_b for creation of electron-buffer-gas ion pairs is due solely to beam electrons and is independent of coordinate.

We show below that metal ions are created, under our conditions, primarily by charge transfer,

[a)]Research supported by the Office of Naval Research.
[b)]Alfred Sloan Foundation Fellow and consultant to NBS (Boulder).

 © 1979 American Institute of Physics

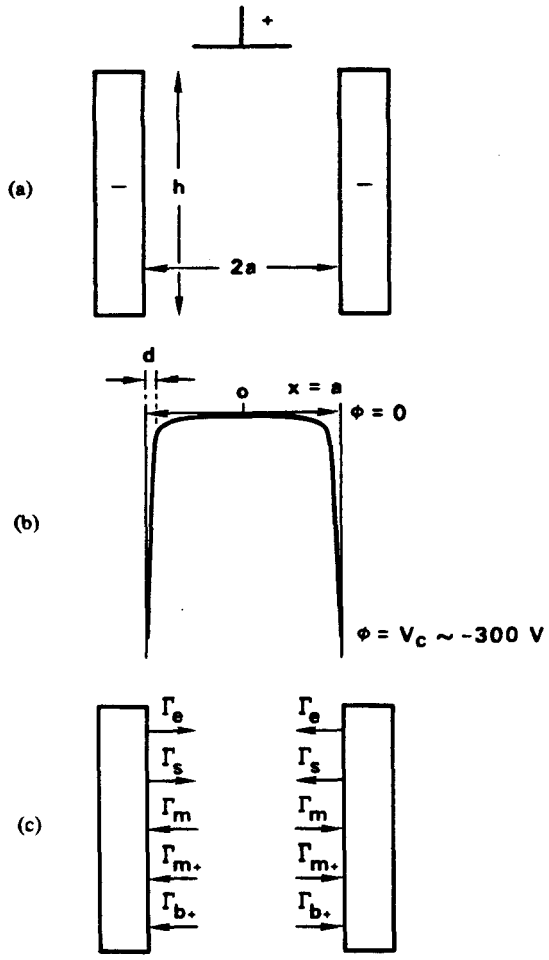

FIG. 1. Cross-sectional view of the plane-parallel hollow cathode and discharge properties. (a) Anode-cathode arrangement. (b) Space potential distribution. (c) Positive directions of flow vectors.

$B^+ + M \rightarrow (M^+)^* + B + \Delta E$, reaction (1), and that the rate of direct ionization of metal atoms is small. The rate of ionization of metal ions by charge transfer can be estimated by

$$R_{CT} = K N_{b.} N_m , \tag{1}$$

where K is the charge-transfer rate constant, $N_{b.}$ and N_m are buffer-gas ion densities and metal-atom densities, respectively.

The ionization rate of both buffer gas and metal ions can be roughly estimated from the current density at the cathode. In the absence of recombination, the total ion flow back to the cathode must be equal to the total ionization rate within the discharge. In detail the ion current at the cathode is related to the current density by various secondary-electron emission coefficients [see Eqs. (14) and (15)]. However, ignoring small differences in these emission coefficients, the ion-flow density at the cathode can be expressed as

$$\Gamma_{\text{ions}} \approx \frac{J}{e(1+\gamma)} , \tag{2}$$

where J is the current density, e is the electronic charge, and γ is the secondary-electron emission coefficient for ion bombardment of the cathode. γ is typically in the range of 0.05–0.1 electrons per ion.[15] Therefore, the total ionization rate (per unit volume) for buffer gas and metal ions is approximately

$$R_{\text{DI}} = \frac{J}{e(1+\gamma)a} , \tag{3}$$

where a is the half-width of the hollow cathode [Fig. 1(a)]. Further assuming that the metal density is low compared to the buffer-gas density, we can estimate the direct ionization rate of the metal ions alone by including the relative densities and ionization cross sections for buffer gas ($Q_{b.}$) and metal atoms ($Q_{m.}$), i.e.,

$$\frac{R_{m.}}{R_{\text{DI}}} = \frac{N_m Q_{m.}}{N_b Q_{b.}} . \tag{4}$$

The ionization rate by charge transfer is found to be 75 times that by direct ionization, using Eqs. (1), (3), and (4) with the following discharge parameters for a Ne-Cu discharge: N_b (1×10^{17} atoms/cm^3), N_m (1×10^{14} atoms/cm^3),[16] $N_{b.}$ (5×10^{13} ions/cm^3),[17] a (1 mm), K (estimate) $= 1\times10^{-9}$ cm^3 sec^{-1}, and $Q_{m.}/Q_{b.} = 5$.[18] This comparison shows almost a hundredfold lower ionization rate of copper ions by direct ionization as compared to charge transfer. Therefore, it is assumed that the metal ions are formed predominately by the charge-transfer process.

Finally, it will be assumed that both recombination and cumulative ionization effects are small. This is done to enable the sputtering model to be phrased in terms of continuity equations and flow densities. It will be seen below that these two processes may, in fact, be incorporated into our model phenomenologically through a gain factor G [see Eq. (8)].

B. Mathematical description

The charge-transfer reaction that populates the upper laser levels is written as

$$B^+ + M \rightarrow B + (M^+)^* + \Delta E,$$

(reaction 1) where B, B^+, and M represent buffer-gas atoms, ions, and metal atoms, respectively. $(M^+)^*$ represents metal ions in an excited energy level, from which the laser action originates and ΔE is the energy defect in the reaction. The reaction rate for this process has been expressed in Eq. (1). By inspecting reaction (1) and Eq. (1), one can see that the presence of charge transfer in the discharge couples the buffer-gas ion density, the metal-vapor density, the metal-ion density, and, thus, the type of ions returning to the cathode. The ions which impinge on the cathode, in turn, produce metal-atom sputtering and secondary-electron emission from the cathode surface.

Our discharge-sputtering model involves integrating the diffusion equations for the various atom and ion species from the center of the discharge to the cathode sheath. This procedure yields a series of coupled flow-density equations for atoms, ions, and electrons at the negative glow-sheath boundary. As pointed out above, the sheath thickness is much smaller than the discharge width, so that the flow-density equations will be assumed valid at the cathode surface. These flow-density equations, together with three others obtained by considering cathode phenomena, will be solved to give the current dependence of the various flow

densities. For the sake of clarity, the flow densities at the cathode, Γ, will be defined as positive in the direction one expects their flow velocity. Figure 1(c) shows the positive directions assumed for the flow-density vectors.

1. Diffusion equations

The spatial dependencies of the metal-atom, and buffer-gas ion densities are determined in the negative-glow region of the discharge by the three diffusion equations

$$D_m \frac{\partial^2 N_m}{\partial x^2} = -S_m + KN_{b.}N_m, \tag{5}$$

$$D_{m.} \frac{\partial^2 N_{m.}}{\partial x^2} = -KN_{b.}N_m, \tag{6}$$

$$D_{b.} \frac{\partial^2 N_{b.}}{\partial x^2} = -S_{b.} + KN_{b.}N_m, \tag{7}$$

where D is a characteristic diffusion coefficient of the species of interest, S is a source function, and N represents density. Only the important source and loss terms as discussed above have been included. The source function for metal atoms, S_m, is due entirely to metal atoms leaving the cathode because of the sputtering. In Sec. III the spatial dependence of $S_m(x)$ will be explored. The buffer-gas ions are assumed to be produced by direct ionization of the buffer-gas atoms by the beam electrons, which originate from the cathode surface. This, together with the assumption of a coordinate independent source function, enables $S_{b.}$ to be expressed as a function of the flow density of electrons leaving the cathode surface,

$$S_{b.} = \frac{G\Gamma_e}{a}, \tag{8}$$

where Γ_e is the flow density of electrons leaving the cathode and G is the number of electron-ion pairs generated in the negative glow per incoming beam electron.[19] G is a quantity that varies with current because of variations in cathode fall, sheath thickness, and atomic densities in the discharge. Note also that the effects of both recombination and cumulative ionization may be incorporated in an effective value of G.

2. Flow-density equations

Instead of solving the coupled nonlinear differential Equations (5) – (7) for the indicated densities, they can be integrated once to yield valuable information at the cathode boundary, such that

$$\Gamma_m = -D_m \frac{dN_m}{dx}\bigg|_{x=a} = \Gamma_s + -K\int_0^a N_{b.}N_m\,dx, \tag{9}$$

$$\Gamma_{m.} = -D_{m.} \frac{dN_{m.}}{dx}\bigg|_{x=a} = K\int_0^a N_{b.}N_m\,dx, \tag{10}$$

$$\Gamma_{b.} = -D_{b.} \frac{dN_{b.}}{dx}\bigg|_{x=a} = G\Gamma_e - K\int_0^a N_{b.}N_m\,dx, \tag{11}$$

where Γ_m is the flow density at the cathode of metal atoms diffusing back to the cathode. $\Gamma_{m.}$ and $\Gamma_{b.}$ are the flow densities at the cathode of metal and buffer-gas ions diffusing back to the cathode, aided by the ambipolar and sheath fields. Γ_s is the result of the integrating S_m over the interval $0-a$ and represents the flow density of metal atoms leaving the cathode due to sputtering. Equation (10) can be used to simplify the other two expressions as follows:

$$\Gamma_s = \Gamma_m + \Gamma_{m.}, \tag{12}$$

$$G\Gamma_e = \Gamma_{b.} + \Gamma_{m.}. \tag{13}$$

Equation (12) can be understood as a continuity equation; the metal atoms that leave the cathode by sputtering must be returned by diffusing back in either atomic or ionic form. Equation (13) relates the rate of return of ions to the cathode to the flow rate of electrons leaving the cthode via the *effective* gain coefficient for production of electron-ion pairs in the negative glow.

3. Cathode phenomena

One can obtain three more balance equations at the cathode surface by considering cathode phenomena. The description of the cathode phenomena, presented below, includes in it an assumption that the cathode-fall voltages does not vary strongly with the current density. Fortunately, this is a reasonable assumption for the sputtering-type hollow-cathode lasers, where cathode-fall voltages increase only 15–20% over an order-of-magnitude increase in current density.[17] Secondary-electron emission coefficients and sputtering yields can then be assumed constant with discharge current density.

The current density at the cathode, J, is easily expressed in terms of the ion and electron-flow densities,

$$J/e = \Gamma_{b.} + \Gamma_{m.} + \Gamma_e, \tag{14}$$

where Γ_e, the flow density of electrons leaving the cathode, is the result of secondary-electron emission due to cathode bombardment of ions, metastables, and photons. It can be expressed as

$$\begin{aligned} \Gamma_e &= \gamma_{b.}\Gamma_{b.} + \gamma_{m.}\Gamma_{m.} + \gamma_p\Gamma_p + \gamma_{\text{met}}\Gamma_{\text{met}}, \\ \Gamma_e &= \gamma_{b.}\Gamma_{b.} + \gamma_{m.}\Gamma_{m.} + \eta G\Gamma_e, \end{aligned} \tag{15}$$

where $\gamma_{b.}, \gamma_{m.}, \gamma_p$, and γ_{met} are the secondary-electron emission coefficients of the cathode material, for bombardment by buffer-gas ions, metal ions, photons, and metastable atoms, respectively. Γ_p and Γ_{met} are flow densities of photons and metastable atoms, which will be assumed to be proportional to the ionization rate in the negative glow. This enables the secondary emission of electrons to be written as it appears in the lower expression of Eq. (15), with η defined as an *effective* coefficient for metastable and photons.

The flow density of sputtered-cathode material, Γ_s, can also be expressed in terms of the ion-flow densities and associated sputtering coefficients $\zeta_{b.}$ and $\zeta_{m.}$ for buffer and metal ions, respectively, i.e.,

$$\Gamma_s = \zeta_{b.}\Gamma_{b.} + \zeta_{m.}\Gamma_{m.}. \tag{16}$$

Each of the sputtering coefficients takes into account the average ion energy upon collision with the cathode surface and are expressed as "atoms liberated per incident ion."

4. Parametric solution

The equation system [Eqs. (12) – (16)] is lacking one

equation to be complete. The missing information can only be obtained by solution of the nonlinear diffusion equations [Eqs. (5) – (7)], which provides three independent equations for the flow densities $\Gamma_m, \Gamma_{m.}$, and $\Gamma_{b.}$, instead of two [Eqs. (12) and (13)]. An approximate solution of Eqs. (5) – (7) will be presented, but a simple parametric solution of the flow-density equations [Eqs. (12) – (16)] can be obtained by introducing a parameter β which is the ratio of buffer-gas-ion to metal-ion flow densities at the cathode surface, i.e.,

$$\beta \equiv \frac{\Gamma_{m.}}{\Gamma_{b.}}. \tag{17}$$

One finds the following equations for the flow densities and G in terms of J/e, β, and the constants $\gamma_{b.}, \gamma_{m.}, \zeta_{b.}, \zeta_{m.}$, and η,

$$\Gamma_{b.} = \frac{1}{(1+\eta)(1+\beta)+\gamma_{b.}+\beta\gamma_{m.}}\frac{J}{e}, \tag{18}$$

$$\Gamma_{m.} = \frac{\beta}{(1+\eta)(1+\beta)+\gamma_{b.}+\beta\gamma_{m.}}\frac{J}{e}, \tag{19}$$

$$\Gamma_s = \frac{\zeta_{b.}+\beta\zeta_{m.}}{(1+\eta)(1+\beta)+\gamma_{b.}+\beta\gamma_{m.}}\frac{J}{e}, \tag{20}$$

$$\Gamma_m = \frac{\zeta_{b.}+\beta(\zeta_{m.}-1)}{(1+\eta)(1+\beta)+\gamma_{b.}+\beta\gamma_{m.}}\frac{J}{e}, \tag{21}$$

$$\Gamma_e \frac{\eta(1+\beta)+\gamma_{b.}+\beta\gamma_{m.}}{(1+\eta)(1+\beta)+\gamma_{b.}+\beta\gamma_{m.}}\frac{J}{e}, \tag{22}$$

$$G = \frac{1+\beta}{(\gamma_{b.}+\eta)+\beta(\eta+\gamma_{m.})}. \tag{23}$$

β can be used as a measure of completeness of the charge-transfer reaction in the discharge. When β is small, most buffer-gas ions have diffused to the cathode without sustaining a charge-transfer collision, but when β is large, the ion current at the cathode is predominantly metal ions because most buffer-gas ions have been converted to metal ions by the charge-transfer process. This is reflected in Eqs. (18) and (19) above. With the total ion current at the cathode defined as

$$\Gamma_+ = \Gamma_{m.} + \Gamma_{b.}, \tag{24}$$

then for $\beta \ll 1$, $\Gamma_{b.} \to \Gamma_+$ and $\Gamma_{m.} \to \beta\Gamma_+$; and for $\beta \gg 1$, $\Gamma_{b.} \to 1/\beta\Gamma_+$ and $\Gamma_{m.} \to \Gamma_+$.

The nature of the sputtering mechanism and how it is influenced by charge transfer can be discerned at this point. Inspecting Eq. (20), when there is little charge transfer in the discharge and $\beta \ll 1$, sputtering is caused primarily by buffer-gas ions and is, therefore, proportional to $\zeta_{b.}$ and the current density. When charge transfer is appreciable and $\beta \gg 1$, sputtering is caused by metal ions and is proportional to $\zeta_{m.}$ and J. The transition between these two regimes is governed by the current dependence of β and the relative sputtering yields for buffer-gas ions and metal ions.

5. Average diffusive lifetime approximation

In order to determine the current dependence of β, a solution of the nonlinear diffusion equations [Eqs. (5) – (7)] must be obtained. This can be done numerically for specific dimensions, diffusion coefficients, and charge-transfer rates but, for the sake of clarity, a phenomenological approach shall be used here. By assuming that the fundamental diffusion mode predominates the diffusion loss of buffer-gas ions and metal atoms to the cathode surface, then $\Gamma_{b.}$ and Γ_m can be formulated in terms of the spatially averaged densities $\bar{N}_{b.}$ and $\bar{N}_m$, and the corresponding average diffusive lifetimes in the discharge, $\tau_{b.}$ and τ_m, i.e.,

$$\Gamma_{b.} = \frac{a}{\tau_{b.}}\bar{N}_{b.}, \quad \Gamma_m = \frac{a}{\tau_m}\bar{N}_m, \tag{25}$$

with

$$\tau_{b.} = \frac{1}{D_{b.}}\left(\frac{2a}{\pi}\right)^2, \quad \tau_m = \frac{1}{D_m}\left(\frac{2a}{\pi}\right)^2, \tag{26}$$

for the geometry of Fig. 1(a). (See Ref. 33, p. 498.) It follows from Eq. (10) that

$$\Gamma_{m.} = aK\bar{N}_m\bar{N}_{b.}. \tag{27}$$

Eliminating the densities between these three equations, we find the relation needed to determine β,

$$\Gamma_{b.}\Gamma_m = \frac{a}{K\tau_{b.}\tau_m}\Gamma_{m.}. \tag{28}$$

By substituting in Eqs. (18), (19), and (21), one finds

$$\frac{K}{a}\tau_{b.}\tau_m\frac{J}{e} = \frac{\beta[(1+\eta)(1+\beta)+\gamma_{b.}+\beta\gamma_{m.}]}{\zeta_{b.}+\beta(\zeta_{m.}-1)}$$

$$\approx \frac{\beta(1+\beta)}{\zeta_{b.}+\beta(\zeta_{m.}-1)}, \tag{29}$$

which relates β to the current density, the diffusive lifetimes $\tau_{b.}$ and τ_m, and the secondary-emission coefficients. As pointed out in Sec. II A, the secondary-electron emission coefficients tend to be very small compared to unity. By ignoring these constants relative to unity, Eq. (29) can be approximated by the lower expression in Eq. (29). Equations (18) – (23) and (29) now specify, within our simplifying assumptions, the current density variations of the five flow densities and the ionization gain factor G. We specifically emphasize that current dependence of sputtering and secondary-emission coefficients have been ignored.

C. Physical interpretation of mathematical description

1. Discussion of relative sputtering yields

The essential features of the sputtering model are contained in Eq. (29), the equation relating β to J. The time constants $\tau_{b.}$ and τ_m can be calculated for specific buffer-gas–metal combinations, buffer-gas pressures, and hollow-cathode dimensions according to Eq. (26). The charge-transfer rate constant K is of the order 10^{-9}–10^{-10} cm^3 sec^{-1} for rare-gas–metal combinations of laser interest.[20] The sputtering coefficients, $\zeta_{b.}$ and $\zeta_{m.}$, warrant some discussion.

Wehner and co-workers[21] have amassed considerable sputtering-yield data for low energy (below 600 eV) rare-gas bombardment of metal surfaces. Their work indicates negligible sputtering yields (less than 10^{-4} atoms/ion)[21] for ions of less than 20 –30 eV. Above 30 eV, sputtering yields exhibit an exponentiallike increase with energy to about 80 –100 eV with yields in the 0.01 – 0.5-atom/ion range.[22] From 80 –110

to 500 eV, the sputtering yield is nearly linear with energy with yields as large as 3 – 4 atoms/ion.[21] Sputtering yields also increase with the mass of the bombarding ion. For instance, argon ions on silver have a sputtering yield of 2.2 atoms/ion at 300 eV, while neon ions on silver at the same energy yield only 1.3 atoms/ion.[23] References 22 and 24 are suggested as reviews of the sputtering-yield measurements and data.

Thus, $\zeta_{b.}$ and $\zeta_{m.}$ must be evaluated using the average incident ion energy and mass. The incident ion energy is likely to be radically different for a buffer-gas ion as compared to a metal ion. This is due to the ion dynamics in the sheath region of the hollow-cathode discharge. The buffer-gas ions undergo resonant charge-transfer collisions with buffer-gas atoms as they traverse the sheath. The mean free path for this collision is in the range 10^{-2}–10^{-4} cm for rare-gas ions of less than 100 eV in 1375 Pa (10 Torr) of the parent gas.[25] Thus the buffer-gas ions upon reaching the cathode will have only a small fraction of the cathode-fall energy; we estimate this energy to be less than 10 eV, depending on the particular gas, pressure, and cathode fall.[26] The metal ions, however, do not suffer nearly as many resonant charge-transfer collisons since the metal-vapor density is 10^{-3}–10^{-4} that of the buffer gas in a sputtering hollow cathode. This results in a resonant charge-transfer mean free path of 1 cm; therefore, the metal-ion mobility is primarily limited by elastic collisions with buffer-gas atoms. Hence, metal-ion energy at the cathode is only slightly less than the cathode fall because the mean free path for momentum-transfer collisions is comparable to the sheath thickness. Typical cathode falls are between 250 and 500 V in a hollow cathode. The effect of this energy difference between buffer-gas ions and metal ions upon the sputtering coefficients is dramatic. Consider, for example, the neon-copper system. Measured sputtering yields for Ne^+ on copper below 10 eV are $\zeta_{Ne^+} < 0.01$ atom/ion.[21] Sputtering yields of Cu^+ on copper are much larger due to the energy and mass difference of the ions. This particular combination has not been measured in the 100 – 500-eV energy range, but is estimated to be slightly larger than Ar^+ on copper. At 300 eV the measured sputtering yield of Ar^+ on copper is about 1.6 atoms/ion.[21] The value of ζ_{Cu^+} should be in the neighborhood of 2 atoms/ion, for a cathode fall of just above 300 V. This represents a factor of 200 difference in ion-sputtering coefficients between Cu^+ and Ne^+ on copper in the hollow-cathode discharge.

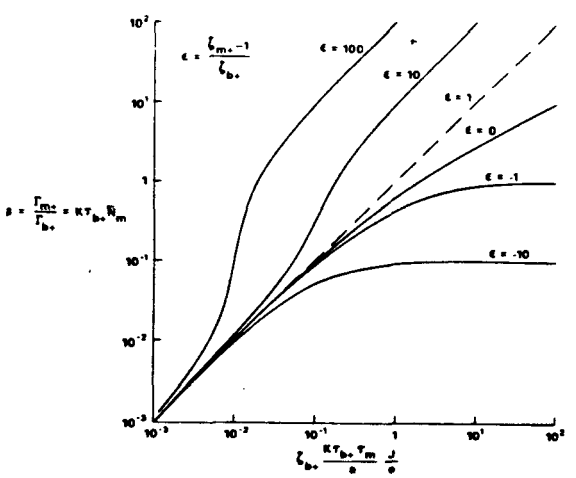

FIG. 2. Dependence of the function β and the metal-vapor density on discharge current density, with ϵ as a parameter; logarithmic scale.

2. Dependence of $\beta = \Gamma_{m.}/\Gamma_{b.}$ on relative sputtering yield

The relative magnitude of the sputtering coefficients, $\zeta_{b.}$ and $\zeta_{m.}$, controls the current dependence of β, the ratio of ion-flow densities at the cathode, in Eq. (29). β also indicates the metal-vapor density in the discharge since, using Eqs. (25) and (28), the metal-vapor density is proportional to β,

$$\bar{N}_m = \frac{\beta}{K\tau_{b.}}. \tag{30}$$

By following the current densities of β, in Eq. (19), for a particular set of sputtering coefficients, one obtains directly the variation of the metal-vapor density with discharge current and an indication of the completeness of the charge-transfer reaction. Further elimination of β from Eqs. (18)–(23) yields the current dependence of the five flow densities and the gain factor G. Since none of these quantities are easily observed, the present analysis shall only consider the current variations of β, the metal density, and the buffer-gas ion density.

The quantity

$$\epsilon = \frac{(\zeta_{m.} - 1)}{\zeta_{b.}} \tag{31}$$

is a useful parameter in scaling Eq. (29) for various ratios of sputtering coefficients. The numerator, $(\zeta_{m.} - 1)$, represents an effective sputtering yield for metal ions. When $\zeta_{m.} = 1$, there are as many metal atoms sputtered from the cathode as metal ions returning to it. In this case only the buffer-gas ions contribute to the production of metal vapor in the discharge.

The function β is plotted versus $[\zeta_{b.}(K/a)\tau_{b.}\tau_m(J/e)]$, a normalized current density, with ϵ as a parameter in Fig. 2. Note there are two solution regions separated by $\epsilon = 1$, which is dashed in Fig. 2. For $\epsilon = 1$, the effective sputtering yield of metal ions is equal to the sputtering yield of buffer-gas ions. When a buffer-gas ion is replaced by a metal ion, due to charge transfer, there is *no net change* in the metal-vapor density. β and $\bar{N}_m$ are then linearly proportional to the current density over the entire current range, as shown by the curve labeled $\epsilon = 1$.

3. Current dependence of β: $\epsilon > 1$

In the solution region above the $\epsilon = 1$ curve, the effective sputtering yield for metal ions *is larger* than the sputtering yield for buffer-gas ions. This results in a net increase in sputtering and metal-vapor density when rare-gas ions are replaced by metal ions because of charge transfer. If ϵ is much larger than unity, β and $\bar{N}_m$ are much different in the low- and high-current-density regimes. For low current density which indicates little sputtering, low metal-vapor density, and insignificant charge transfer, Eq. (29) yields

$$\beta_{\text{low}} = K\tau_{b.}\bar{N}_m \cong \zeta_{b.}\left(\frac{K}{a}\tau_{b.}\tau_m\frac{J}{e}\right), \quad \beta < \frac{1}{\epsilon}. \tag{32}$$

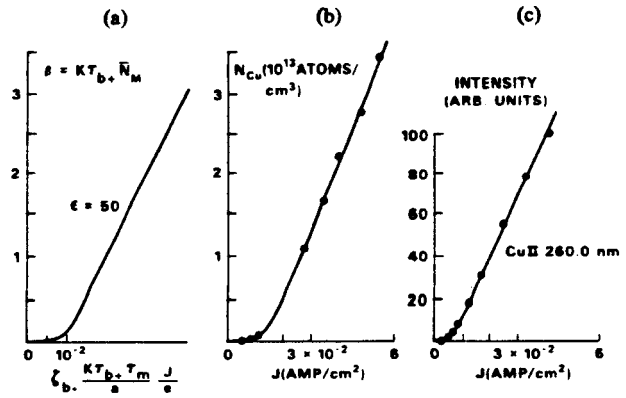

FIG. 3. Dependence of the function β and the metal-vapor density on discharge current density; linear scales. (a) Plot of β versus current density for $\epsilon = 50$. (b) Measurements of copper vapor density versus discharge current density. (From Ref. 16.) (c) Measurements of Cu II 260.0-nm intensity versus discharge current density. (From Ref. 17.) The upper level of this transition is populated by charge transfer from Ne^+.

For high current density, when there is appreciable sputtering, higher metal-vapor density, and significant charge transfer,

$$\beta_{\text{high}} = K\tau_{b.}\bar{N}_m \simeq (\zeta_{m.} - 1)\left(\frac{K}{a}\tau_{b.}\,\tau_m\,\frac{J}{e}\right), \quad \beta > 1\,. \tag{33}$$

Thus, it is seen that β and $\bar{N}_m$ are linearly proportional to the current density in both the high- and low-current-density regimes, but rises nonlinearly with the current density in the transition region, defined by

$$1/\epsilon < \beta < 1. \tag{34}$$

As illustrated in Fig. 2, β and $\bar{N}_m$ increase in the transition region with approximately the fourth power of the current density for $\epsilon = 100$. For $\epsilon = 10$, they are roughly proportional to the second power of the current density.

The transition region has a very distinctive effect on β and $\bar{N}_m$ when plotted on linear (in contrast to logarithmic in Fig. 2) scale. This is illustrated in Fig. 3(a) and shows that for high values of ϵ, the linear portion of the β and $\bar{N}_m$ curves do *not* intersect the origin. Instead, it appears as if the sputtering process has a current density threshold. This apparent threshold arises from the transition from low-sputtering-yield buffer-gas ions to high-sputtering-yield metal ions via the charge-transfer process, reaction (1).

4. Current dependence of β: $\epsilon < 1$

The solution region below $\epsilon = 1$ in Fig. 2 corresponds to the situation in which the effective sputtering coefficient for the metal ions $(\zeta_{m.} - 1)$ is less than the buffer-gas ion sputtering coefficient, $\zeta_{b.}$. In this case, the replacement of a buffer-gas ion by a metal ion, because of the charge transfer, reduces the net metal-vapor density in the discharge. It is conceivable that a particular metal ion may have a sputtering coefficient of less than unity, resulting in a negative ϵ. For $\epsilon < 0$, β and $\bar{N}_m$ are linearly porportional to the current density for low current density since the sputtering is caused primarily by the buffer-gas ions. As the current density increases, the current dependence of β and $\bar{N}_m$ becomes sublinear because metal ions start to replace buffer-gas ions, and eventually β and $\bar{N}_m$ saturate and become independent of the current density. The high current limiting value of β is

$$\beta_{\text{limit}} = K\tau_{b.}\bar{N}_m = \frac{\zeta_{b.}}{(\zeta_{m.} - 1)} = -\frac{1}{\epsilon}, \quad \epsilon < 0\,. \tag{35}$$

For large negative ϵ, β is very small, indicating little charge transfer and low metal-vapor density, regardless of the current density.

5. Current dependence of buffer-gas ion density

Since the charge-transfer reaction converts buffer-gas ions to metal ions, it is reasonable to ask what the buffer-gas ion density $\bar{N}_{b.}$ is doing in the different current density regimes. Solving Eqs. (18), (25), and (29) $\bar{N}_{b.}$ has the parametric form

$$\zeta_{b.}K\tau_m\bar{N}_{b.} = \frac{\beta}{1 + \beta\epsilon}\,. \tag{36}$$

By numerical elimination of β between Eqs. (36) and (29), one finds the current density variation of $\bar{N}_{b.}$, as plotted in Fig. 4. For negative values of ϵ, the buffer-gas ion density is only slightly perturbed by the sputtering and charge transfer at high current densities. The most interesting features of the $\bar{N}_{b.}$ behavior are for positive value of ϵ. The buffer-gas ion density starts out increasing linearly with the current density, but enters a sublinear regime, corresponding to the transition regions in Fig. 2. Eventually the buffer-gas ion density *saturates* when the charge-transfer loss rate $K\bar{N}_{b.}\bar{N}_m$ equals the ionization rate $S_{b.}$. The saturation value is obtained by taking the limit of large β in Eq. (36),

$$\bar{N}_{b.} = \frac{1}{K\tau_m(\zeta_{m.} - 1)}, \quad \beta \gg 1\,. \tag{37}$$

This value is reached only for β much larger than unity and near complete charge transfer.

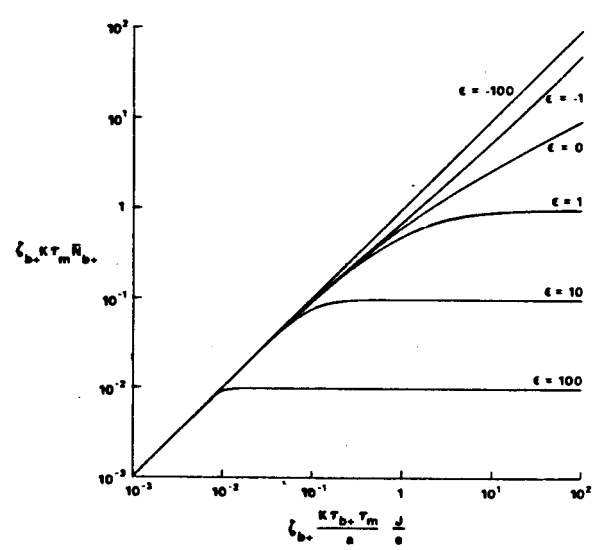

FIG. 4. Dependence of buffer-gas ion density on discharge current density, with ϵ as a parameter; logarithmic scale.

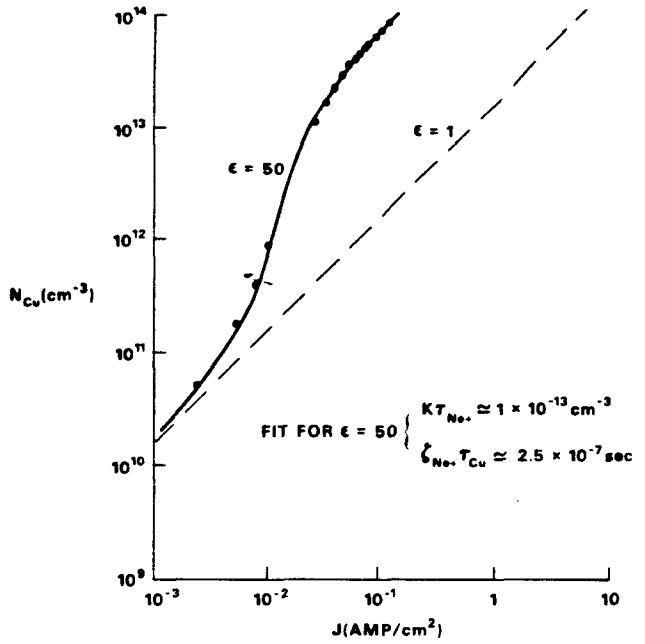

FIG. 5. Dependence of copper-vapor density on discharge current density for the neon-copper system. The data points are measurements. (From Ref. 16.) The solid line is a fit from the discharge-sputtering theory, with parameters as indicated.

D. Experimental data

Measurements have been made on the discharge properties in a Ne-Cu hollow-cathode discharge by de Hoog *et al.*,[1] McNeil,[16] and Vaessen.[15] The discharge properties measured include copper density, spatial profile of copper density, electron temperature, ion and neutral temperatures, metastable densities, and electron density. The technique for copper density and metastable measurements has been that of fractional absorption using Gaussian[27] or Voight[28,29] profiles for atomic line shapes. The Voight-profile analysis yields roughly a factor of 4 higher absolute densities[30] than the Gaussian analysis. Below we select data from all of these sources which used similar hollow-cathode conditions and geometries to compare with our theory.

Figure 5 contains the copper density measurements collected by Vaessen[16] (Voight analysis) at 1000 Pa (7.5 Torr) neon which we have plotted on a scale similar to Fig. 2. By choosing the effective sputtering-yield ratio ϵ equal to 50 and adjusting the axes, our theory is seen to fit the data over three orders of magnitude. A choice of ϵ equal to 100 or 10 would produce a transition region that is either too abrupt or too slow to fit the data; the agreement at $\epsilon = 50$ is remarkable considering the approximations used to arrive at Eq. (29). The axes adjustment on the log-log plot yields directly the two parameters found in Fig. 5, $K\tau_{Ne^+}$ and $\zeta_{Ne^+}\tau_{Cu}$. By using the fundamental diffusion mode formulas [Eqs. (26)] and appropriate diffusion coefficients,[32,33] the time constants are $\tau_{Cu} \simeq 1.5 \times 10^{-5}$ sec and $\tau_{Ne^+} \simeq 5 \times 10^{-5}$ sec for $a = 1$ mm. These can be used along with the parameters from the data fit to obtain the charge-transfer rate coefficient for Ne^+ with Cu and the sputtering yields, ζ_{Ne^+} and ζ_{Cu^+}. $K_{Ne^+\text{-}Cu}$ is found to be 2×10^{-9} cm^3 sec^{-1}, within a factor of 4 of typical values.[20] The sputtering yields are found to be $\zeta_{Ne^+} \simeq 1.7 \times 10^{-2}$ atoms/ion and $\zeta_{Cu^+} \simeq 1.85$ atoms/ion, consistent with the estimates in Sec. II C 1.

As predicted by our theory, the copper density varies linearly with current density at *both* high and low currents. It is noteworthy that, as discussed previously, in the low-current region the copper vapor is produced by neon-ion sputtering, whereas, at high current the copper vapor is produced primarily by copper-ion sputtering. The change from neon ions to copper ions via reaction (1) causes the observed nonlinearity. This same data, plotted on a linear scale, is found in Fig. 3(b).

The observed intensity of spontaneous emission from upper laser levels of Cu II is plotted in Fig. 3(c) as a function of discharge current.[1] Two distinguishing features of Fig. 3(c) are the apparent threshold and the linearity at high current. This linear behavior with current is also seen in the laser output.[17] One expects that since charge transfer is the dominant excitation mechanism of upper Cu II lase levels, both the laser and the spontaneous-emission intensities would vary according to Eq. (1). That is, the output should be proportional to the product of the ground-state neutral-copper density times the ground-state neon-ion density. Therefore, the only self-consistent interpretation of the measured results in Figs. 3(b) and 3(c) is that the density of ground-state neon ions saturates with increasing current in agreement with our theory. (See Fig. 4.)

In summary, our discharge-sputtering model is in good agreement with experimental data despite the approximations outlined earlier. However, to unambiguously determine the suitability of this model both the copper- and neon-ion densities should be measured as a function of current to display both the change in ion species, as well as the saturation of neon-ion density due to charge transfer, reaction (1).

III. SPATIAL VARIATION OF METAL DENSITY

A. Introduction

Metal-vapor densities as a function of position have been measured by the fractional-absorption techniques with a resolution of 0.15 mm.[16,17] It is therefore important to extend our model to include the spatial variations of metal-vapor density, as well as metal-vapor density variations due to changes in buffer-gas pressure. Unfortunately this behavior is buried in the coupled nonlinear differential equations [Eqs. (5) – (7)]. Knowing the current dependence of the average metal-vapor density and its physical significance, we can make reasonable approximations to Eqs. (5) – (7), so that they become tractable in the limit of high ($\beta \gg 1$) metal-vapor density. This is the most intersting limit because the charge-transfer lasers operate only in this region.[17]

The diffusion equations for the density of both the metal atoms and buffer-gas ions in a hollow-cathode discharge are given in Eqs. (5) and (7), respectively. In these equations the source functions S_b and S_m are quite different. S_b is independent of position due to the approximation discussed previously in Sec. II A. However, S_m is known to vary with position since the metal atoms originate at the wall as a beam[31] and subsequently thermalize with the buffer gas as they enter the discharge. This description of a spatially ex-

tended source for metal vapor is necessary because the diffusion equation cannot describe the nonthermal transport of the sputtered metal atoms. Measured most probable ejection energies of sputtered atoms tend to be in the 1–5 V range, dependent upon metal and ion species, but surprisingly independent of ion energy.[31] This ejection energy is at least an order of magnitude higher than the buffer-gas temperatures in sputtering hollow-cathode lasers.

The approach we employ is to use an exponentially decreasing, normalized source function from each cathode surface. In the geometry of Fig. 1(a) this results in a source function of the form

$$S_m = \Gamma_s \frac{\cosh(x/l)}{l \sinh(a/l)}, \tag{38}$$

where the characteristic length l, $l(=1/N_b Q)$, is the thermalization length for the atom beam in the buffer gas and Q is the momentum-transfer cross section for the metal atom with the buffer gas. For very high buffer-gas densities, the energetic metal atoms thermalize very close to the cathode and S_m then resembles a delta function at the cathode surface. For very low buffer-gas densities, the metal-atom source function may extend a significant distance into the discharge according to Eq. (38).

B. Spatial profiles: theory, $\beta > 1$ region

For high current and metal-vapor density ($\beta > 1$), Eqs. (5) – (7) can be solved approximately. Subtracting Eq. (7) from Eq. (5) eliminates the charge-transfer term. The resulting equation is

$$D_m \frac{\partial^2 N_m}{\partial x^2} - D_{b.} \frac{\partial^2 N_{b.}}{\partial x^2} = -S_m + S_{b.}. \tag{39}$$

This can be integrated directly,

$$N_m - \frac{D_{b.}}{D_m} N_{b.} = \frac{\Gamma_s l}{D_m}\left(\frac{\cosh(x/l)}{\sinh(a/l)}\right) + \frac{\Gamma_e G}{2D_m}\left(\frac{x^2}{a}\right) + C.$$

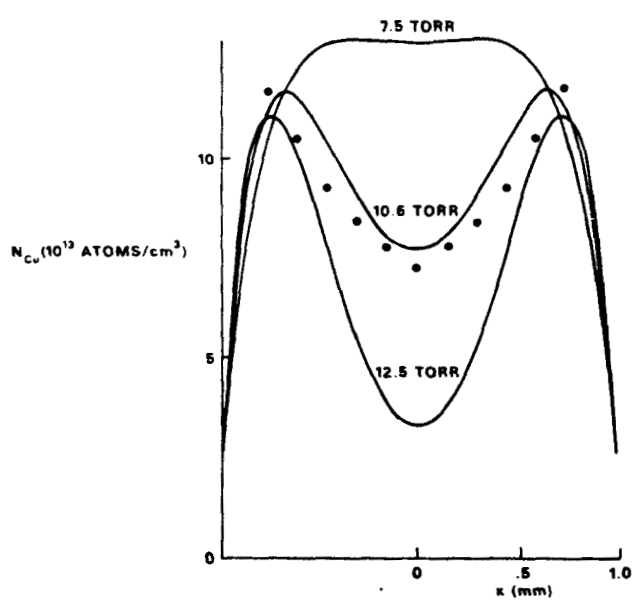

FIG. 6. Spatial dependence of copper-vapor density on buffer-gas pressure at a constant current in the high-current region ($\beta > 1$, $J = 0.2$ A/cm^2). The data points are measurements (from Ref. 17) at 1400 Pa (10.6 Torr) Ne, scaled up to be consistent with data of Ref. 16. See text for discussion.

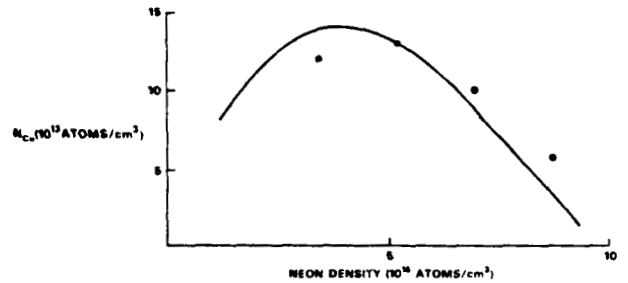

FIG. 7. Dependence of copper-vapor density at the center of the discharge on neon buffer-gas density at fixed current. ($\beta > 1$, $J = 0.2$ A/cm^2.) The solid line is from the discharge-sputtering theory. The data points are from Ref. 16.

At this point the buffer-gas ion density term is dropped. The ratio of the diffusion coefficient is of order unity, but for $\beta > 1$; the buffer-gas ion density has saturated, in accordance with Eq. (37), at a density *small* compared to the metal-vapor density. This approximation is equivalent to saying the buffer-gas ion loss in Eq. (7) is determined by charge transfer and not diffusion. For high β this is a good approximation except very near the cathode, where the sheath fields will aid the diffusion, and for very high pressures when the metal-vapor density in the center of the discharge may drop to values of the same order as $\bar{N}_{b.}$. For both of these cases the buffer-gas ion diffusion term must be considered in the solution of Eq. (40).

The constant C in Eq. (40) is obtained by applying a boundary condition on N_m at the cathode surface. The metal-atom flow density Γ_m gives us the required information

$$N_m(a) = \frac{\Gamma_m}{v_t} \simeq \frac{1}{v_t}\left(-D_m \frac{\partial N_m}{\partial x}\bigg|_{x=a}\right), \tag{41}$$

where v_t is the velocity of the thermal metal atoms diffusing back to the cathode. This results in

$$N_m = \frac{\Gamma_s l}{D_m \sinh(a/l)}[\cosh(a/l) - \cosh(x/l)] + \frac{\Gamma_e G}{2D_m a}(x^2 - a^2) + \frac{\Gamma_m}{v_t}. \tag{42}$$

Note that the spatial profile maintains its functional form with increasing current since Γ_s, Γ_e, and Γ_m are all linearly proportional to J in the limit of high β. The changes which do occur with increasing current arise primarily through small changes in the characteristic constants D_m, l, and G, due to increased buffer-gas temperatures and cathode-fall voltages. Equation (42) is plotted in Fig. 6, with coefficients applicable to a Ne-Cu discharge, at 0.2 A/cm^2, as in Refs. 1, 16, and 17.

Equation (42) also contains information concerning the variation of metal density with buffer-gas pressure. This can best be seen by evaluating N_m at $x = 0$ and recognizing that according to simple kinetic theory, $l = 1/QN_b$ and $D_m = (1/N_b)(v/3Q)$,

$$N_m(x=0) = \frac{\Gamma_s[\cosh(aQN_b) - 1]}{Q(v/3Q)\sinh(aQN_b)} - \frac{\Gamma_e G a N_b}{2(v/3Q)} + \frac{\Gamma_m}{v_t}. \tag{43}$$

Figure 7 is a plot of $N_m(0)$ versus N_b for the same current density as in Fig. 6. In the low N_b limit Eq. (43) can be simplified by a power-series expansion of the hyperbolic terms. This yields a linear dependence of the metal density with buffer-gas density. The decrease of metal density at low buffer-gas densities is due to the increased loss of metal atoms due to increased diffusion loss.

In the high N_b limit the hyperbolic terms in Eq. (43) are large and their ratio approaches unity, causing the first term to approach a constant, $\Gamma_s/Q\,(v/3Q)$. Hence, the overall dependence of the metal density with N_b is linear, but with a *negative* slope equal to $\Gamma_e Ga[2(v/3Q)]^{-1}$. Figure 7 displays both the low and high N_b limits as well as the transition region. At very large N_b, the metal-vapor density appears to cross zero and go negative. This is obviously incorrect. The problem can be traced to our assumption, above, that the buffer-gas ion density is small compared to the metal-vapor density. When the metal-vapor density approaches the buffer-gas ion density, buffer-gas ion diffusion must also be considered because charge transfer is no longer the dominant loss for the buffer-gas ions in the center of the discharge. This is expected to cause N_m to go to zero asymptotically in a more complete mathematical analysis.

C. Experimental data

Spatially resolved (0.15 mm) metal-atom density measurements have been made on the hollow-cathode discharges of interest.[1,16,17] Since the lasers operated in the region $\beta > 1$, we present the corresponding data (Gaussian analysis) in Fig. 6 for comparison with our theoretical results. Note that only the relative and not the absolute value of the data should be compared to our theoretical curves because of the uncertainty in the absolute metal-atom density arising from line-shape considerations in the absorption measurements as discussed previously.[27–30] Note, also, that the theoretical profile of Fig. 6 is sensitive to the value of the diffusion coefficient of the metal atom in the buffer gas.[33]

The measured variation of the copper density at $x = 0$ and at fixed discharge current is plotted in Fig. 7. Note the close agreement between the data and our crude model. Again the discharge conditions were $J = 0.2$ A/cm^2 and the buffer gas was neon at the indicated density. This data is taken from the Voight analysis of Vaessen.[16]

IV. SUMMARY AND CONCLUSIONS

The measured metal density and its spatial variation in a hollow-cathode discharge compare favorably with our discharge-sputtering model which is based on the following assumptions: One, the sputtering of metal atoms is caused by both rare-gas ions and metal ions impinging on the cathode surface; two, the sputtering yields of metal ions and rare-gas ions may differ by several orders of magnitude; and three, the densities of rare-gas ions, metal-vapor ions, and metal-vapor atoms are coupled via the charge-transfer reaction, reaction 1. As a consequence, the discharge current *cannot* be independently varied or optimized with respect to the desired metal-vapor density. Finally, the competition between charge-transfer and diffusion loss gives rise to a spatially nonuniform metal-atom density which peaks near the cathode surfaces. Our theory predicts the observed central minimum in metal-atom density and the measured variation of this minimum with buffer-gas density.

A surprising prediction of our discharge-sputtering model is the saturation of the neon-ion density at current densities in excess of 0.03 A/cm^2 (see Sec. II C) in the Ne-Cu system. Our spontaneous-emission[1] and laser output power[17] studies versus current density, in the region above 0.03 A/cm^2, apparently confirm this predicted behavior. The saturation of neon-ion density is shown to arise predominantly from the loss of neon ions in the charge-transfer process, reaction (1). In summary, to a first approximation, because both the rate of production and the rate of loss of neon ions is proportional to current, the neon-ion density saturates above 0.03 A/cm^2.

Since the production of metal-ion energy levels which support laser oscillation depends upon the product of the rare-gas ion density times the neutral-metal density, as in Eq. (1), the ion saturation as described above has two consequences. First, the charge-transfer rate to the upper level of the laser transition is linear with discharge current. Second, an increase in metal density at *fixed* current density will not increase the output power because the saturated rare-gas ion density will be decreased proportionally via the charge-transfer process.

It is important to note that our model assumes that the rate of production of buffer-gas ions by the beam electrons is *not* affected by increased metal density. This assumption is justified providing the electron impact ionization of the metal vapor is small compared to the direct ionization of the buffer gas, see Eq. (4). Therefore, it is expected that the charge-transfer rate, which in the region of saturated buffer-gas ion density is proportional to the ionization rate of the buffer gas, will remain linearly proportional to the current density until the ratio, in Eq. (4), approaches unity.

The metal-ion lasers, designed around the sputtering technique,[2–10] represents a new type of practical device. Discharge sputtering produces metal densities in excess of 10^{14} atoms/cm^3.[1,16] To achieve equivalent metal densities thermally, a temperature in excess of 1,300 °C is required. Moreover, such cathodes operate at room temperature, a considerable practical advantage. These lasers have been shown to provide 0.1–1 W of single line output power.[10] Remarkably, the laser transitions, in the He-Ag laser for example, span the entire optical region from 0.2 to 2.0 μm.[5,6,34]

ACKNOWLEDGMENTS

The authors would like to thank J.R. McNeil, F.S. deHoog, and R. Reid for helpful discussions, and J. Cooper for a critical reading of the manuscript.

[1] F.S. de Hoog, J.R. McNeil, G.J. Collins, and K.B. Pearsson, J. Appl. Phys. **48**, 3701 (1977).
[2] L. Csillag, M. Janossy, K. Rozsa, and T. Salamon, Phys. Lett. A **50**, 13–14 (1974).
[3] J.R. McNeil, G.J. Collins, K.B. Persson, and D.L. Franzen, Appl. Phys. Lett. **27**, 595–598 (1975).
[4] J.R. McNeil, G.J. Collins, K.B. Persson, and D.L. Franzen, Appl. Phys. Lett. **28**, 207–209 (1976).
[5] W.L. Johnson, J.R. McNeil, G.J. Collins, and K.B. Persson, Appl. Phys. Lett. **29**, 101–102 (1976).

[6]J.R. McNeil, W.L. Johnson, G.J. Collins, and K.B. Persson, Appl. Phys. Lett. **29**, 172–174 (1976). For a discussion of unidentified Ag-II lines see R.D. Reid, D.C. Gerstenberger, J.R. McNeil, and G.J. Collins, J. Appl. Phys. **48**, 3994 (1977).
[7]D.C. Gerstenberger, R.D. Reid, and G.J. Collins, Appl. Phys. Lett. **29**, 466 – 468 (1977).
[8]R.D. Reid, J.R. McNeil, and G.J. Collins, Appl. Phys. Lett. **30**, 666 – 668 (1976).
[9]W.K. Schuebel, Appl. Phys. Lett. **30**, 516 –519 (1977).
[10]B.E. Warner, D.C. Gerstenberger, R.D. Reid, J.R. McNeil, R. Solanki, K.B. Persson, and G.J. Collins, IEEE J. Quantum Electron. **QE-14**, 568 (1978).
[11]W.K. Schuebel, in *Proc. XI Int. Conf. Phenomena in Ionized Gases* (Czech. Academy of Science, Prague, 1973), p. 174.
[12]P. Gill and C. Webb, J. Phys. B **10**, 299 (1977).
[13]K.B. Persson, J. Appl. Phys. **36**, 3086 (1965).
[14]P.F. Little and A. Von Engel, Proc. R. Soc. London A **224**, 109 (1954).
[15]S.C. Brown, *Basic Data of Plasma Physics* (Wiley, New York, 1959), p. 222.
[16]P. Vaessen, M. Eng. thesis, Technical University of Eindhoven, 1978.
[17]J.R. McNeil, Ph.D. thesis, Colorado State University, 1976.
[18]For Cu, C.K. Crawford, Particle Optics Laboratory, MIT Tech. Report No. 1, AFML-TR-67-376, 1967. For Ne, D. Rapp and P. Englander-Golden, J. Chem. Phys. **43**, 1464 (1965).
[19]Lennart R. Peterson, Phys. Rev. **27**, 105 (1969).
[20]A.R. Turner-Smith, J.M. Green, and C.E. Webb, J. Phys. B **6**, 114 (1973).
[21]N. Laegrid and G.K. Wehner, J. Appl. Phys. **32**, 365 (1961).
[22]G.K. Wehner and G.S. Anderson, in *Handbook of Thin Film Technology*, edited by I. Maissel and R. Glang (McGraw-Hill, New York, 1970), Chap. 3.
[23]D. Rosenberg and G.K. Wehner, J. Appl. Phys. **30**, 1842 (1962).
[24]L.I. Maissel, in *Physics of Thin Films*, edited by G. Hass and R. Thun, Vol. 3, p. 61 (Academic, New York, 1971), Vol. 3, p. 61.
[25]W.H. Cramer and J.H. Simone, J. Chem. Phys. **26**, 1272 (1957).
[26]B.E. Warner, Ph.D. thesis, University of Colorado, 1979.
[27]R. Ladenburg and F. Reiche, Ann. Phys. N.Y. **42**, 181 (1913).
[28]Y. Fugol, D. Myshkis, and O. Grigorashchenko, Opt. Spectrosc. (U.S.S.R.) **31**, 282 (1971).
[29]I. Kato, A. Iwasake, A. Adachi, and T. Shimizu, J. Opt. Soc. Am. **68**, 1008 (1978).
[30]P. Vaessen, F.J. De Hoog, and J.R. McNeil, Phys. Lett. A **68**, 204 (1978).
[31]R.V. Stuart and G.K. Wehner, J. Appl. Phys. **35**, 1819 (1964) and R.V. Stuart, G.K. Wehner, and G.S. Anderson, J. Appl. Phys. **40**, 803 (1969).
[32]The ambipolar diffusion coefficient for neon ions in neon gas at 1300 Pa (10 Torr) Ne and 1300 °K is $D_{Ne^+} \approx 71$ cm^2 sec^{-1}, from H.J. Osakam and V.R. Mittelstadt [Phys. Rev. **132**, 1435 (1963)].
[33]The diffusion coefficient used for copper atoms in a neon buffer gas at the same pressure and temperature is $D_{Cu} \approx 200$ cm^2 sec^{-1}, consistent with values obtained from an elastic sphere model as in: E.W. McDaniel, *Collision Phenomena in Ionized Gases* (Wiley, New York, 1964), p. 50.
[34]R. Solanki (private communication).